INTERSTITIAL FLOW INSTABILITIES DURING STEADY-STATE TWO-PHASE FLOW IN MICROFLUIDIC PORE NETWORK MODELS

N. Karadimitriou[1], M.S. Valavanides[2,*], H. Steeb[1]

[1] nikolaos.karadimitriou@mechbau.uni-stuttgart.de, University of Stuttgart
[1] holger.steeb@mechbau.uni-stuttgart.de, University of Stuttgart
[2] marval@uniwa.gr, University of West Attica
* marval@uniwa.gr

ABSTRACT

In an on-going systematic laboratory study we examine the applicability of a recently proposed flow-rate dependent relative permeability scaling model in describing immiscible two-phase flows in artificial 2D microfluidic networks, across different flow regimes and for different wetting /non-wetting fluid systems. The scope is to assess the potential of inherent characteristic invariants of the scaling model in revealing the interstitial flow structure from external (ex-network) measurements.

We constructed a Poly-Di-Methyl-Siloxane (PDMS) pore network micromodel. We used a fluorine-based fluid, acting as the wetting phase, and water as the non-wetting phase. We run steady-state, two-phase flow experiments, by co-injecting the two phases at different flow rates, in order to scan an extended domain of flow conditions in terms of capillary number and flowrate ratio. For every run under fixed flowrate conditions, we keep track of the evolution of the pressure drop, measured between the inlet of each phase and the common outlet, until dynamic equilibrium settles-in. In addition, we keep track of the interstitial flow structure by taking snapshots at appropriate frame rates.

During the simultaneous injection of both fluids at constant flowrates, the evolution of the wetting and nonwetting phase pressures at the inlets is associated to a transitory reconfiguration of the interstitial flow. That happens from the onset of injection to the point where dynamic equilibrium eventually settles-in. In particular we have recorded pressure fluctuations at the wetting and non-wetting pahse inlets and we present how these evolve with time as the process attains a fully developed interstitial flow structure. As said, the (co-)injection of the two immiscible liquids is maintained at constant flowrates. Nevertheless, we observe different modes of fluctuation of the measured pressures at the two inlets. The time evolution of these pressure fluctuations show different types of attenuation, from underdamped, through critically damped, to overdamped, indicating an underlying, systematic interstitial response of the system, to externally imposed flow conditions (capillary number and flowrate ratio).

KEYWORDS: two-phase flow, microfluidc network, pressure fluctuations, instabilities

1. INTRODUCTION

The conventional use of saturation as the independent variable in two-phase flows in porous media (PM) is based on the assumption that relative pemeabilities, i.e. terms accounting for the flow resistances in the momentum balance, can be correlated to a volumetric average quantity (saturation). The assumption is correct when considering the flow resistance terms due to bulk viscosity. Nevertheless, the resistance to the flow depends also on capillarity and the associated hysteresis effects, which, on their term, depend on the degree of disconnection of the NWP. The latter depends on the imposed flow conditions, for any given set of the physicochemical properties of the fluids/matrix system and the geometry of the pore network.

Flow conditions in steady-state, two-phase flow in pore networks have an adverse effect on the momentum balance. In particular, on the relevant magnitude of the Stokes flow resistances due to the bulk viscosity of the NWP and WP, and to Young-Laplace resistances, due to the contact forces between the N/W menisci and the pore walls. The former depend on local (micro /pore scale) velocity gradients, in contrast to the latter that are relatively independent of the displacement rates of the menisci. From an energy point of view, the power dissipation, due to bulk viscosity, scales with the square of the local velocity gradients, whereas the capillarity-induced dissipation scales with the rates of displacement of the menisci. For relatively low values of the superficial velocity, viscosity effects are insignificant compared to capillarity effects; as flow intensity is progressively increasing, viscosity takes over from capillarity and the flow progressively mutates from capillarity-dominated to transient capillarity/viscosity- to viscosity-dominated characteristics [1]. In that context, especially at moderate/low superficial velocities and, in particular, when capillary forces are comparable to viscous forces, the macroscopic pressure gradient does not scale linearly with the flow rate. Experimental studies on steady-state two-phase flows in glass beads, in glass bead columns, as well as in sand-pack columns, revealed that the non-linear relation between the pressure gradient and the flow rate can be described by generic power laws with different exponent values [1]. The discrepancy between the values of the scaling exponents may be attributed to differences associated with the dimensionality of the pertinent variables, measurements pertaining to different flow conditions, dimensionality of the NWP/WP/PM system etc. These 'different' observations can be integrated in a universal power law relating appropriate, dimensionless variables of the process [2].

In an on-going laboratory study we examine aspects of flow-rate dependency of relative permeabilities when immiscible steady-state, two-phase flow takes place within artificial 2D microfluidic networks, across different flow regimes. The general scope is to assess the applicability and/or universality of the aforementioned scaling function across NWP/WP/PM systems of different sizes, and to examine the forensic character of the kernel function, i.e. the potential for revealing the interstitial flow structure. Just recently, we concluded the first part of the aforementioned laboratory study [3]. Data were collected over a grid of specially selected flow conditions, spanning 4 orders of magnitude over the capillary number, *Ca*, and up to 3 orders of magnitude over the flow rate ratio, *r*. The study is conceptually similar to that performed recently within a natural core (sandstone) [4], albeit it was performed in a microfluidic network with direct visualization of the interstitial flow structure.

In the course of the lab study, we have observed a systematic behavior during concurrent injection of both phases at fixed volumetric fluxes: pressure fluctuations were measured at the inlet of both immiscible phases; their characteristics (period, decay time, phase difference) seem to depend on the flow conditions. In an effort to provide an overview of a -presumably systematic- underlying phenomenology, we present indicative diagrams of the time evolution of the observed fluctuations over a broad domain of flow conditions.

2. METHODOLOGY

The laboratory study presented here comprises the simultaneous, continuous, steady-state, co-current injections of two inniscible fluids, within a specially prepared microfluidic network, and for a variety of flow conditions, by adjusting the flow rates (volumetric fluxes), $\tilde{q}_n$ and $\tilde{q}_w$, of the NWP and WP respectively. That includes 152 experimental runs in total, organized in 13 groups of constant capillary number values. The capillary number is conventionaly defined as $Ca = \tilde{\mu}_w \widetilde{U}_w / \tilde{\gamma}_{nw}$, where $\widetilde{U}_w = \tilde{q}_w / \tilde{A}$ is the superficial velocity (or flowrate intensity), $\tilde{A}$ is the cross sectional surface area of the pore network (perpendicular to the superficial flow direction), $\tilde{\mu}_w$ is the dynamic viscosity of the NWP, and $\tilde{\gamma}_{nw}$ is the interfacial tension between the NWP and WP. The flowrate ratio is defined as, $r = \tilde{q}_n / \tilde{q}_w$. The entire set of runs, spans ~4 orders of magnitude over *Ca* and ~3 orders over *r*.

2.1 Microfluidic Model and Fluids

A Poly-Di-Methyl-Siloxane (PDMS) micromodel was used as the pore network. It was produced in-house, following the principles of optical and soft lithography [5]. The pore structure of the micromodel is depicted in Fig. 1(A). The effective dimensions of the pore space are 10mm×20mm. The constant depth of the porous structure is 43 μm. The pore network is periodic in both principal orthogonal directions on a 3×2 tiling-up of a basic network element along the longitudinal and across the transverse axis. The pore size range is [75-250] μm, with a mean size of 180 μm.

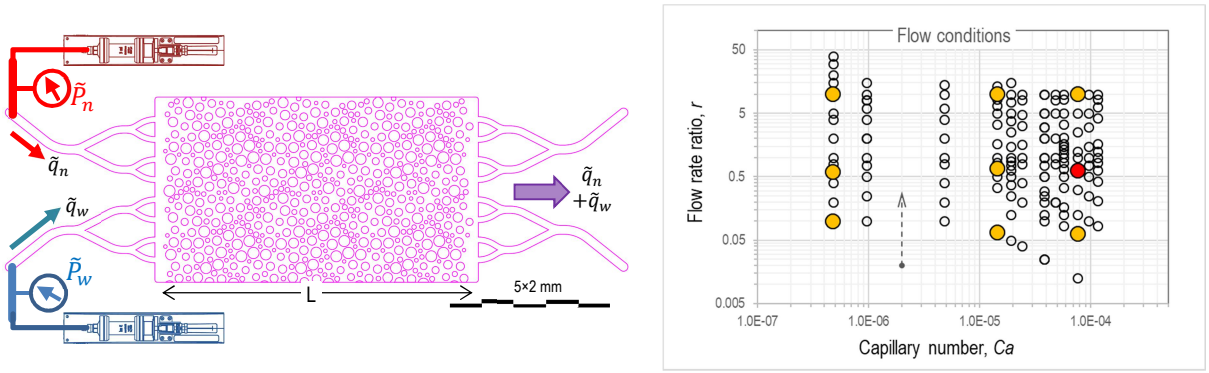

Figure 1: (A) Plane section of the microfluidic PDMS network with physical dimensions 20mm×10mm×43μm. Circles correspond to PDMS matrix elements (pillars connecting the two parallel plates confining the flow). The fluids are simultaneously injected at predetermined, fixed volumetric flowrates. (B) The domain of steady-state flow conditions examined in the study. Circular markers indicate values of the capillary number, Ca, and the flow rate ratio, r, examined per constant-Ca experiment. The arrow indicates the progressive increase of the flowrate of the NWP per experiment (at fixed Ca). The solid markers (yellow & red) identify flow conditions pertaining to the time evolution diagrams in Fig.2

Table 1: Basic physicochemical properties of the fluids used in the study

Fluid	Density, $\tilde{\rho}$ [Kg/m^3]	Dynamic viscosity, $\tilde{\mu}$ [mPas]	Interfacial tension $\tilde{\gamma}_{nw}$ [N/m]
Fluorinert^{TM} FC-770 (WP)	1793	1.35	55×10^{-3}
Deionized Water + Dye (NWP)	1000	1.00	

The cross sectional surface area (perpendicular to the superficial flow direction) is $\tilde{A} = 4.3 \times 10^{-7}\mathrm{m}^2$. The measured absolute permeability, taking into account the inlet/outlet network, is $\tilde{k} = 8.1 \times 10^{-1}\ \mathrm{m}^2$. The two immiscible fluids are injected through the inlet micro-channeling on the left side of the network. The immiscible flow exits through the outlet micro-channeling on the right side, Fig. 1(B).

In the set of experiments presented here, the fluids used were deionized water dyed with ink, as the non-wetting phase (NWP), and Fluorinert^{TM} FC-770, as the wetting phase (WP). Their properties are presented in Table 1. We verified by measurements that the addition of dye in water had practically no effect on viscosity and density.

2.2 Experimental Set-up and Procedure

For the simultaneous injection of the fluids, at independent volumetric fluxes, two CETONI^{TM}, neMESYS 1000N, syringe pumps were used, one for each fluid, Fig. 1(A). The syringe pumps were combined with a BASE120 module. With this set-up it was possible to inject the fluids at volumetric fluxes as low as a few microliters per minute, to maintain a capillarity-dominated flow regime, up to milliliters per minute (ml/min) to sustain viscosity-dominated flow regimes. The inlet pressure of each phase was measured using various types of Elveflow^{TM} MPS sensors, depending on the values of the expected pressure build-up during the injection and the desirable /acceptable measurement accuracy. Both syringe pumps, and logging of the pressure readout values were controlled with QMixElements^{TM}.

The entire flow system was visualized using an open-air microscope harnessed with a single camera, instead of four, as a modification of a previous layout [6]. The camera used is a Basler™ 5 Mpx, 23 fps, acA2440-20gm, monochrome camera. With the direct visualization of the interstitial flow, it was possible to check the structure of the flow and compare it to the read-outs from the pressure transducers and the injected fluxes, and figure-outthe degree to which the process has reached a steady state fully developed interstitial structure. There was no video recording but simple snapshot capturing.

Procedure followed for each experiment – With the term "experiment" we refer to a complete cycle of co-injecting the two phases, at different values of the flowrate ratio, *r*, but maintaining a constant value of the capillary number, *Ca*. Within a constant *Ca* experiment, the volumetric flux of the NWP is sequentially increased in successive steps. In that context, a set of flowrate ratio values, *r*, spanning across 0.1 to 10 is administered for every fixed *Ca* value experiment. The domain of flow conditions in the entire set of experiments is depicted in Fig. 1(B).

The typical cycle in every experiment comprises the following interventions:

- The micromodel is initially saturated with the WP. Then,
- Both phases are co-injected into the microfluidic network; the WP is injected at a fixed volumetric flux in order to maintain a constant *Ca* value, during the entire cycle of the experiment. The NWP/WP volumetric flux ratio starts at ~1/10 and increases in (9-10) successive steps to 10.
- After each step-up of the NPW flux, an adequate period of time is allowed for the flow to reach steady-state. As soon as the time-averaged pressure values showed signs of stabilization for both phases, the entire microfluidic network is visually inspected to verify that the interstitial flow is also stabilized, allowing also for sustainable, short-cycle periodicity, depending on flow conditions.
- Upon establishment of fully developed conditions, the flux of the NWP is stepwise increased.
- Successive repetitions? with stepwise increments of the flux of the NWP, will eventually reach a flow rate ratio of $r = 10$. Then, the experiment for that particular constant *Ca* set stops.
- The system is then reconfigured to accommodate the next cycle pertaining to a new *Ca* (q_w) value.

For every run, the displacement pumps maintain the immiscible flow at constant flowrates. That maintains a constant value of the flowrate ratio, which, by definition, $r = \tilde{q}_n/\tilde{q}_w$, is a kinematic variable – as it depends on the externally imposed "geometric aspects" of the flow. On the other hand, the mobility ratio is, by definition, $\lambda = k_{rn}/(\kappa k_{rn})$, a kinetic variable – it consists of the relative permeabilities which on their term, describe the momentum balance over the geometric aspects of the flow, i.e. the macroscopic velocities and the disconnection of the NWP. The two mobiliies are equal only when fully developed conditions have settled-in [1].

2.3 Data logging and management

For each run at constant $\tilde{q}_n$ and $\tilde{q}_w$, the values of flow rates and gauge pressures at the inlet ports for each phase were sampled and recorded, at acquisition rates between 0.5 and 10 Hz, depending on the flow conditions.The recorded data were graphically plotted. End-point pressures were estimated from these plots by time averaging, over an adequate time length of sampling (see next section).

The typical procedure is depicted in the diagrams in Fig. 2, on which the time evolution of the two flow rates and pressures at the inlets are displayed. Please note that, the time axis (horizontal) and the flux axis (vertical, right) are logarithmic whereas the pressure axis (vertical, left) is linear. Pressure values are indicated by markers; fluxes are indicated by lines. The endpoint pressure values are calculated by time averaging over a selected interval. The selected time interval is delimited by the two "×" markers. Delimiting this time interval for every examined flow set-up, (Ca, r), follows after identifying some form of stabilization in the corresponding pressure

diagram. The average end-point pressures $\langle \tilde{P}_n \rangle, \langle \tilde{P}_w \rangle$, are calculated by simple averaging over the selected time interval. Then, pressure gradients for the WP and the NWP are calculated as $(\Delta\tilde{p}/\Delta\tilde{z})_i = \langle \tilde{p}_i \rangle / L\,, i = n, w$. The corresponding pair of relative permeability values for the NWP and WP is calculated as $k_{ri} = \tilde{\mu}_i \tilde{U}_i / \left[\tilde{k}(\Delta\tilde{p}/\Delta\tilde{z})_i\right],\ i = n, w$.

3. RESULTS & DISCUSSION

The pressure fluctuations at the WP and NWP inlets evolve with time as the process attains an almost fully developed interstitial flow structure, from the onset of injection to the point where dynamic equilibrium settles-in. An overview of the pressure evolution for indicative flow conditions is presented in the diagrams of Fig. 2. The diagrams are tabulated on a 3×3 layout. Each column pertains to constant-*Ca* experiments, $Ca \sim 4.8 \times 10^{-7},\ 1.4 \times 10^{-7},\ 7.7 \times 10^{-5}$, i.e. for capillarity-dominated, capillary/viscous and viscosity-dominated flows respectively. Each row pertains to injections at equivalent flowrate ratios, $r \sim 0.07,\ 0.7,\ 10$. The flow conditions presented in Fig.2 are those marked in the diagram in Fig. 1(b) by solid markers (in yellow and red color).

In most cases, stabilization of the inlet pressures comes along with a stabilized flow, judging from visual inspection of the interstitial flow (changes in saturation, migration of menisci, other pore-scale phenomena). Occasionally, for low volumetric fluxes of the NWP, i.e. low *Ca* values, we observe periodic fluctuations and/or oscillations over the pressure readouts for both phases, which are always accompanied with snap-off events within the pores. In these cases, the system is left to oscillate for a few periods, so as to identify the characteristics of the oscillation, e.g. actual period and wavelength (see indicative diagrams in Fig. 2, left column, bottom).

Overall, we observe a systematic behavior, showing different degrees of attenuation. That indicates dynamic similarities to a multimodal spring/damper/mass oscillating system. In that context, the interstitial flow oscillations are due to the interplay between: (a) the densities of the two fluids; (b) the relative magnitudes of the Young-Laplace forces exerted by the NWP/WP menisci; (c) the energy dissipation due to the viscosities of the NWP and WP, as well as the hysteretic behavior of the menisci -due to differences on the dynamic advancing and receding contact angles within the atypical network geometry. The interplay is regulated /biased by the geometry of the pore network. The attenuation of the intertitial flow oscillations can vary from underdamped, through critically damped, to overdamped, indicating the response of the system depends on the changes, or perturbations, in the externally imposed flow conditions. We may infer that these different modes of attenuation and system response would also depend on the viscosity ratio of the system.

In general our observations are in line with those reported in a recent work on interstitial flow fluctuations in natural cores [7]. The systematic structure of the intertitial flow oscillations indicate the potential for applications in flow and NWP/WP/PM system characterization, e.g. ex-core flow characterization, rock typing etc. A possible research direction to follow is to perform a Fourrier analysis of the pressure evolution, and correlate it to the flow conditions and the physicochemical properties of the system.

ACKNOWLEDGEMENTS

M.S. Valavanides would like to thank (a) the German Academic Exchange Service (DAAD - 5752335 Research Stays for University Academics and Scientists, 2021), (b) the Society of Petrophysicists and Well Log Analysts (SPWLA Foundation Board, 2021 award), (c) the University of West Attica.

N. Karadimitriou and H. Steeb would like to thank the Deutsche Forschungsgemeinschaft (DFG) for supporting this work by funding EXC2075-390740016 under Germany's Excellence Strategy, as well as the DFG for supporting this work by funding of Sonderforschungsbereich (SFB) 1313 project 327154368.

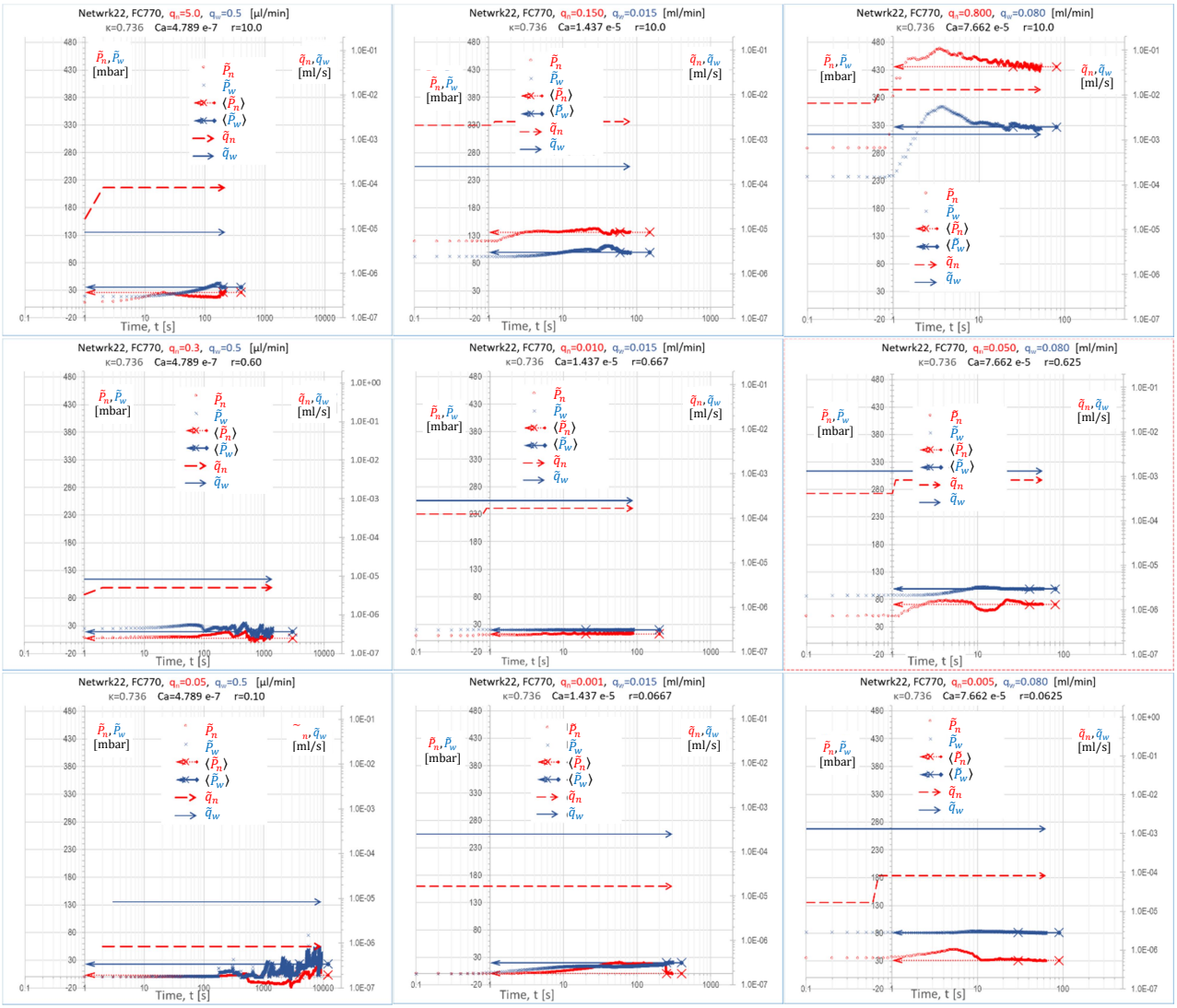

Figure 2: Time evolution of the inlet pressure for typical co-injections of the two phases at different predetermined volumetric flow rates. (Flow conditions pertain to those indicated in the diagram Fig.1(B) by the solid markers.) Compact line (blue, ▬) indicates the volumetric flow rate for the WP, $\tilde{q}_w$, dashed line (red, ▬ ▬) for the NWP, $\tilde{q}_n$, (the step indicates the imposed increase in volumetric flow rate succeeding the previous co-injection set-up). The time evolution of the measured pressure at the inlet port of the NWP is indicated by the small circle markers (red, ○); the pressure evolution at the WP inlet port is indicated by the small cross markers (blue, ×). The arrows facing the left axis indicate the pressure values reached when steady-state conditions settle-in. (see main text for details).

REFERENCES

[1] Valavanides, M.S. (2018). *Transport in Porous Media*, 123 (1): 42-99. DOI: 10.1007/s11242-018-1026-1

[2] Valavanides, M.S. (2018). *Proceedings of the International Symposium of the Society of Core Analysts*, paper SCA2018-066, Trondheim, Norway, 27-30 Aug. http://users.uniwa.gr/marval/publ/Valavanides_SCA2018_066.pdf

[3] Valavanides, M.S., Karadimitriou, N., & Steeb, H. (2022). *SPWLA 63rd Annual Logging Symposium*, 0054, Stavanger, NO, Jun. 11-15, DOI: 10.30632/SPWLA-2022-0054, http://users.uniwa.gr/marval/publ/Valavanides_etal_2022_SPWLA63_0054c.pdf

[4] Valavanides, M.S., Mascle, M., Youssef, S., & Vizika, O. (2020). *E3S Web of Conferences*, 146 (03002) *The International Symposium of the Society of Core Analysts, SCA2019*. DOI: 10.1051/e3sconf/202014603002

[5] Xia, Y., & Whitesides, G.M. (1998). *Annu. Rev. Mat. Sci.* 28, 153-184. DOI: 10.1146/annurev.matsci.28.1.153

[6] Karadimitriou, N. K., Musterd, M., Kleingeld, P. J., Kreutzer, M. T., Hassanizadeh, S. M., & Joekar-Niasar, V. (2013). *Water Resources Research* 49: 2056–2067. DOI: 10.1002/wrcr.20196.

[7] Rücker, M., Georgiadis, A., Armstrong, R.T., Ott, H., Brussee, N., van der Linde, H., Simon, L., Enzmann, F., Kersten, M. & Berg, S. (2021). *Frontiers in Water* 3 (671399): 1-25. DOI: 10.3389/frwa.2021.671399